ARHGEF17 is an essential spindle assembly checkpoint factor that targets Mps1 to kinetochores

Mayumi Isokane,[1] Thomas Walter,[1] Robert Mahen,[1] Bianca Nijmeijer,[1] Jean-Karim Hériché,[1] Kota Miura,[2] Stefano Maffini,[3] Miroslav Penchev Ivanov,[4] Tomoya S. Kitajima,[1] Jan-Michael Peters,[4] and Jan Ellenberg[1]

[1]Cell Biology and Biophysics Unit and [2]Centre for Molecular and Cellular Imaging, European Molecular Biology Laboratory, 69117 Heidelberg, Germany
[3]Department of Mechanistic Cell Biology, Max Planck Institute of Molecular Physiology, 44227 Dortmund, Germany
[4]Molecular and Cellular Biology, Research Institute of Molecular Pathology, 1030 Vienna, Austria

To prevent genome instability, mitotic exit is delayed until all chromosomes are properly attached to the mitotic spindle by the spindle assembly checkpoint (SAC). In this study, we characterized the function of ARHGEF17, identified in a genome-wide RNA interference screen for human mitosis genes. Through a series of quantitative imaging, biochemical, and biophysical experiments, we showed that ARHGEF17 is essential for SAC activity, because it is the major targeting factor that controls localization of the checkpoint kinase Mps1 to the kinetochore. This mitotic function is mediated by direct interaction of the central domain of ARHGEF17 with Mps1, which is autoregulated by the activity of Mps1 kinase, for which ARHGEF17 is a substrate. This mitosis-specific role is independent of ARHGEF17's RhoGEF activity in interphase. Our study thus assigns a new mitotic function to ARHGEF17 and reveals the molecular mechanism for a key step in SAC establishment.

Introduction

Faithful chromosome segregation requires that sister chromatids attach their kinetochores to opposite poles of the mitotic spindle. To prevent genome instability, mitotic exit is delayed by the spindle assembly checkpoint (SAC; Rieder et al., 1994; Rieder and Salmon, 1998; Alexandru et al., 1999; Musacchio and Salmon, 2007; Musacchio, 2011; Foley and Kapoor, 2013) until all kinetochores are correctly bioriented. The core SAC machinery undergoes enzymatic and/or conformational activation at kinetochores to form the mitotic checkpoint complex (Musacchio and Salmon, 2007; Lara-Gonzalez et al., 2012), which prevents mitotic exit by inhibiting the anaphase-promoting complex/cyclosome (APC/C) and E3 ubiquitin ligase.

An essential regulator of the checkpoint machinery is the mitotic kinase Mps1 (Weiss and Winey, 1996; Hardwick et al., 1996; Abrieu et al., 2001; Stucke et al., 2002; Jelluma et al., 2008a; Santaguida et al., 2010). Mps1 activity directs checkpoint proteins to unattached kinetochores (Lan and Cleveland, 2010), allows Mad2 conformational activation (Hewitt et al., 2010), and stabilizes the cytoplasmic APC/C inhibitory complexes (Maciejowski et al., 2010). It thereby prevents the cell cycle from prematurely advancing from metaphase to anaphase before attachment of every chromosome to spindle microtubules (Abrieu et al., 2001; Stucke et al., 2002). In the absence of Mps1 activity, the SAC is constitutively inactivated, and cells therefore become rapidly aneuploid and subsequently die (Kops et al., 2005). Mps1 activity rises during mitosis (Stucke et al., 2002), when it becomes localized to kinetochores (Howell et al., 2004) and is autoactivated by cross-phosphorylation of its activation loop (Kang et al., 2007; Jelluma et al., 2008b) as a dimer (Hewitt et al., 2010). Although the essential function of Mps1 to establish the SAC has been reported in many model systems (Hardwick et al., 1996; Weiss and Winey, 1996; He et al., 1998; Abrieu et al., 2001), it is not understood how Mps1 is targeted to kinetochores and how the cell ensures that the right amount of Mps1 activity is present at kinetochores during mitosis.

Here, we functionally characterize ARHGEF17, an essential mitotic gene, identified in the MitoCheck genome-wide RNAi screen (Neumann et al., 2010). ARHGEF17 was originally identified as a guanine nucleotide exchange factor (GEF) of the Rho GTPase family, with a function in regulation of the interphase cytoskeleton (Rümenapp et al., 2002). ARHGEF17 is a 2,063-aa-long protein, and only its 187-aa GEF domain is

Correspondence to Jan Ellenberg: jan.ellenberg@embl.de

R. Mahen's present address is Photonics Group, Dept. of Physics, Imperial College London, London SW7 2AZ, England, UK.

T. Walter's present address is Centre for Computational Biology, Mines ParisTech, Fontainebleau 77300, France; Institut Curie, Paris 75248, France; and U900, Institut National de la Santé et de la Recherche Médicale, Paris 75248, France.

T.S. Kitajima's present address is RIKEN Center for Developmental Biology, Kobe 650-0047, Japan.

Abbreviations used in this paper: ACA, anti-centromere antibody; APC/C, anaphase-promoting complex/cyclosome; BAC, bacterial artificial chromosome; FCCS, fluorescence cross correlation spectroscopy; FL, full length; GEF, guanine nucleotide exchange factor; IEX, ion exchange chromatography; LAP, localization and affinity purification; LC-MS/MS, liquid chromatography-tandem mass spectrometry; SAC, spindle assembly checkpoint.

The Rockefeller University Press $30.00
J. Cell Biol. Vol. 212 No. 6 647–659
www.jcb.org/cgi/doi/10.1083/jcb.201408089

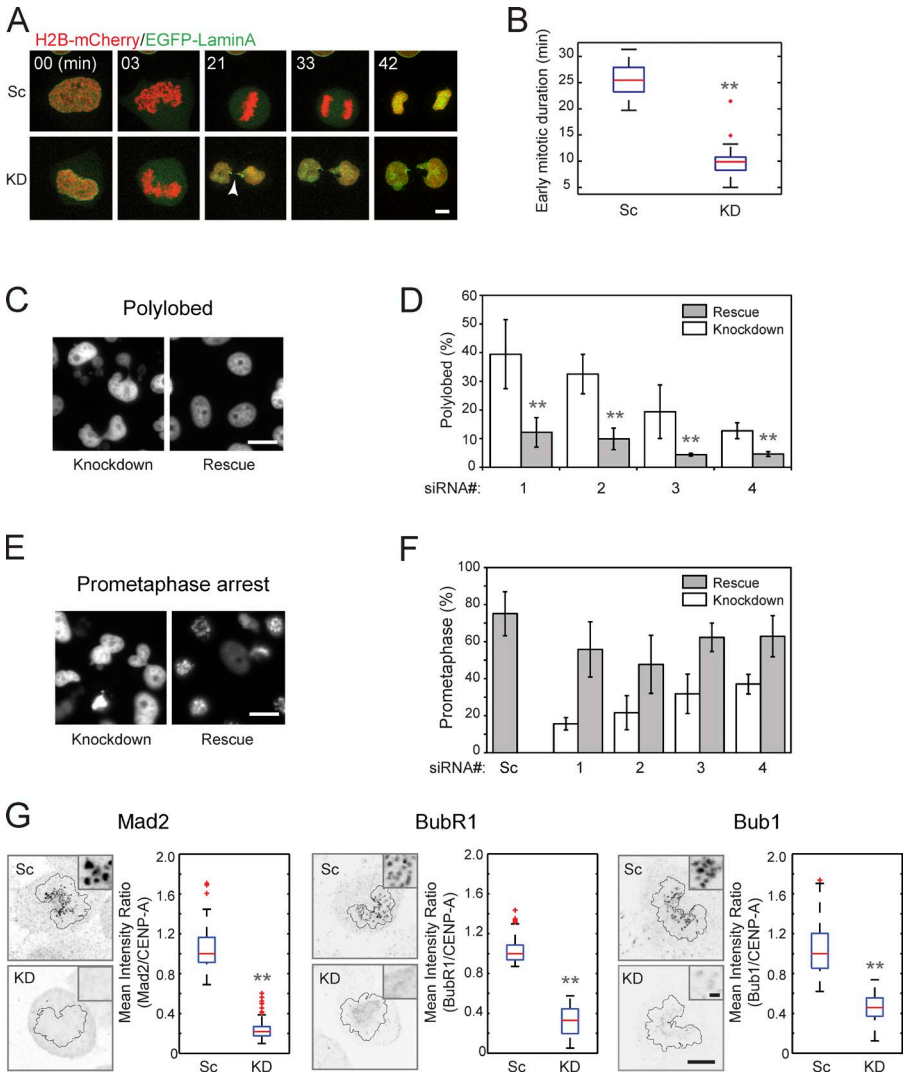

Figure 1. **ARHGEF17 is required for SAC.** (A and B) Knockdown (KD) of hARHGEF17 in HeLa Kyoto cells stably expressing H2B-mCherry and EGFP-laminA. (A) Time series of cells treated with si(Scrambled) (Sc) or si(hARHGEF17) (KD). Arrowhead marks a chromosome bridge. (B) Comparison of early mitotic duration (prometaphase + metaphase) from >22 mitosis/three independent experiments. (C and D) Validation of siRNA targeting of hARHGEF17 by phenotypic rescue through LAP-mARHGEF17-BAC. (C) Nuclei (H2B-mCherry) 48 h after siRNA transfection with or without LAP-mARHGEF17-BAC rescue. (D) Comparison of polylobed nuclei populations (normalized to Scrambled in each condition) from >6,000 cells/three independent experiments. siRNA number indicated (see Materials and methods). (E and F) SAC activity of ARHGEF17. (E) Nuclei (H2B-mCherry) treated with 0.33 µM nocodazole 48 h after siRNA transfection with or without LAP-mARHGEF17-BAC rescue. (F) Comparison of cell populations in prometaphase of >4,500 cells/three independent experiments. siRNA number indicated. (G) Quantitative expression analysis of checkpoint proteins at kinetochores in prometaphase. (left) Localization of Mad2, BubR1, or Bub1 after Scrambled or hARHGEF17-KD. (inset) High magnification of kinetochores. Black lines outline segmented chromosomes. (right) Comparison of mean intensity ratio between checkpoint proteins and CENP-A at >1,300 individual sister kinetochores/three independent experiments. Bar graphs show mean ± SD; boxes show median, 25–75%; whiskers show 1.5× interquartile range. Bars: (A and G) 5 µm; (G, inset) 0.5 µm; (C and E) 10 µm. **, $P < 0.01$ by two-tailed unpaired Student's *t* test, compared with si(Scrambled) (B and G) or without a rescue construct (D).

functionally annotated. A mitotic function of ARHGEF17 had not been reported before MitoCheck. Here, we demonstrate that ARHGEF17 is essential for the SAC and for targeting Mps1 to mitotic kinetochores, that the ARHGEF17–Mps1 interaction is regulated by Mps1 kinase activity, and that ARHGEF17 is a substrate of Mps1 kinase. We propose a model in which the autoregulated ARHGEF17–Mps1 targeting complex acts as a timer to ensure the correct level of Mps1 activity for SAC function at kinetochores.

Results

ARHGEF17 is a human mitotic gene

ARHGEF17 was discovered as a mitotic hit in the MitoCheck RNAi screen because of its polylobed nuclear phenotype (Neumann et al., 2010). Because polylobed nuclei can arise owing to several mitotic defects that were not captured with the time resolution of the genome-wide screen, we assayed this phenotype in more detail with high-resolution confocal time-lapse imaging of chromosomes (H2B-mCherry) and the nuclear envelope (laminA-mEGFP). Dividing HeLa cells depleted for ARH GEF17 showed dramatically accelerated mitosis and proceeded directly from prometaphase to anaphase, without detectable chromosome congression and biorientation in metaphase, so that anaphase onset occurred on average 9.1 (± 4.8) min after nuclear envelope breakdown, compared with 25.4 (± 3.0) min in control cells (Fig. 1, A and B). Consequently, chromosome segregation was highly abnormal, leading to prominent chromosome bridges, explaining the formation of polylobed nuclei after segregation (Fig. 1 A, arrow). The dramatic mitotic acceleration and complete skipping of metaphase suggest that the SAC is severely compromised in the absence of ARHGEF17.

To confirm ARHGEF17 as the siRNA target gene responsible for the phenotype, we next performed phenotypic rescue with an RNAi-resistant ARHGEF17 transgene, using the mouse orthologue of ARHGEF17 in a bacterial artificial chromosome (BAC; mARHGEF17; Poser et al., 2008), stably expressed in a HeLa cell line with fluorescently labeled chromosomes (H2B-mCherry). The on-target knockdown was efficient, as endogenous hARHGEF17 protein was reduced by >80% after knockdown with four independent human-specific siRNAs in both parental and mARHGEF17-expressing HeLa cells (Fig. S1 A). Time-lapse imaging and quantitation of mitotic phenotypes in cell populations by automatic classification of chromosome morphologies using CellCognition (Held et al., 2010; Walter et al., 2010; http://www.cellcognition.org, see Materials and methods) confirmed a significant increase of

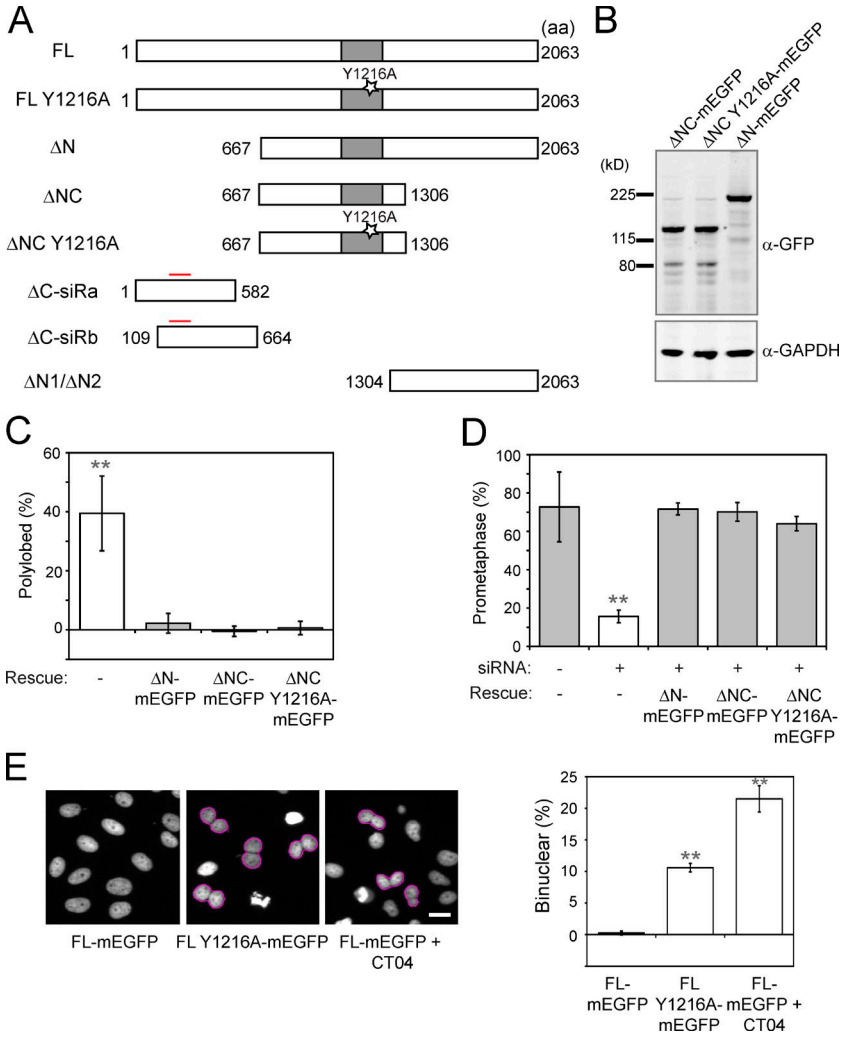

Figure 2. **ARHGEF17 fragment restores SAC function independently of catalytic activity for Rho GEF of ARHGEF17.** (A) Schematic depiction of hARH GEF17 variants used in phenotypic rescue assays: FL: hARHGEF17 (1–2,063)-mEGFP; FL Y1216A: hARHGEF17 (1–2,063)-Y1216A-mEGFP; ΔN: hARH GEF17 (667–2,063)-mEGFP; ΔNC: hARHGEF17 (667–1,306)-mEGFP; ΔNC Y1216A: hARHGEF17 (667–1,306)-Y1216A-mEGFP; ΔC-siRa: hARH GEF17 (1–582)-mEGFP; ΔC-siRb: hARHGEF17 (109–664)-mEGFP; ΔN1: mEGFP-hARHGEF17 (1,304–2,063)-mEGFP; and ΔN2: hARHGEF17 (1,304–2,063)-mEGFP. Gray boxes indicate GEF activity domain (Dbl-homologous domain); Y1216A indicates the inactivating mutation in the GEF domain; red lines indicate sites for mutations for siRNA resistance. (B) Immunoblot analysis of hARHGEF17 fragments fused to GFP (detected with anti-GFP). GAPDH, loading control. (C and D) Rescue of hARHGEF17 knockdown-induced polylobulation (C) or SAC defect (D). Comparison of polylobed (C; normalized to Scrambled) or prometaphase population (D; nocodazole treated) rescued with hARHGEF17 fragments (ΔN-mEGFP, ΔNC-mEGFP, and ΔNC Y1216A-mEGFP) of >11,500 (C) or >6,300 (D) cells/three independent experiments. (E) Phenotypic analysis of cytokinesis defects (binucleation) of a catalytically inactive mutant of full-length ARHGEF17 (FL Y1216A) during mitosis. (left) H2B-mCherry, wild-type full-length (FL-mEGFP), catalytically inactive (FL Y1216A-mEGFP), or cells 24 h after CT04 treatment (0.25 mg/ml; FL + CT04). (right) Comparison of binuclear population of >3,000 cells/three independent experiments. Bar graphs show mean ± SD. **, $P < 0.01$ by two-tailed unpaired Student's *t* test, compared with no rescue construct (C), si(Scrambled) without a rescue construct (D), or FL-mEGFP (E). Cells automatically segmented/analyzed by CellCognition. Bars, 10 µm.

polylobed nuclei after ARHGEF17 knockdown with all siRNAs, indicative of failed chromosome segregation (Fig. 1, C and D). For all siRNAs, expression of the siRNA-resistant mARH GEF17 significantly reduced the abundance of polylobed nuclei (Fig. 1 D). To confirm that this phenotypic rescue was indeed caused by mARHGEF17 and not other sequences present on the BAC rescue construct, we performed double knockdown of both human and mouse ARHGEF17 by two siRNAs, which restored the polylobed phenotype, demonstrating that the rescue was specific to mARHGEF17 (Fig. S1 B). ARHGEF17 is therefore a bona fide human mitotic gene.

ARHGEF17 is required for the SAC

The mitotic acceleration phenotype of ARHGEF17 knockdown suggests that it is required for the SAC. We therefore tested whether ARHGEF17 depletion would abolish the checkpoint-dependent cell cycle arrest induced by the microtubule-depolymerizing drug nocodazole. Whereas a large fraction of control cells treated with nocodazole arrested in prometaphase, only very few cells depleted of ARHGEF17 were found in prometaphase after drug treatment (Fig. 1 E). This checkpoint override was rescued by the siRNA-resistant mARHGEF17 transgene for all four siRNAs targeting hARHGEF17 (Fig. 1 F). Because overall protein expression of hMad2 was not affected by ARHGEF17 knockdown (Fig. S2 A) and a mouse Mad2 orthologue construct could not rescue the ARHGEF17 knockdown phenotype (and vice versa; Fig. S2, B and C), we excluded the possibility of off-target gene silencing of hMad2 by hARH GEF17 siRNAs, previously reported for other gene targets (Hübner et al., 2010; Westhorpe et al., 2010; Sigoillot et al., 2012). The expression levels of other checkpoint proteins such as BubR1 and Bub1 were also not affected by ARHGEF17 knockdown (Fig. S2 D). Thus, ARHGEF17 is specifically required for the SAC.

ARHGEF17 localizes to kinetochores and is required for targeting of checkpoint and outer kinetochore proteins

Given that the SAC operates at kinetochores, we next investigated the subcellular distribution of endogenous ARH GEF17 during mitosis using immunofluorescence with anti-ARHGEF17 antibodies. In dividing HeLa cells, endogenous ARHGEF17 localized to the mitotic spindle, the cytoplasm, and the kinetochores (Fig. S2 E). Since even the best available antibody showed relatively weak kinetochore labeling over the cytoplasmic background, we confirmed the kinetochore localization on chromosome spreads from cells arrested in prometaphase with nocodazole, where endogenous ARHGEF17 prominently localized to the centromere/kinetochore region (Fig. S2 F), consistent with a function in the SAC.

To understand how ARHGEF17 is required for SAC function, we tested whether its depletion affects the kinetochore targeting of checkpoint proteins, which has been shown

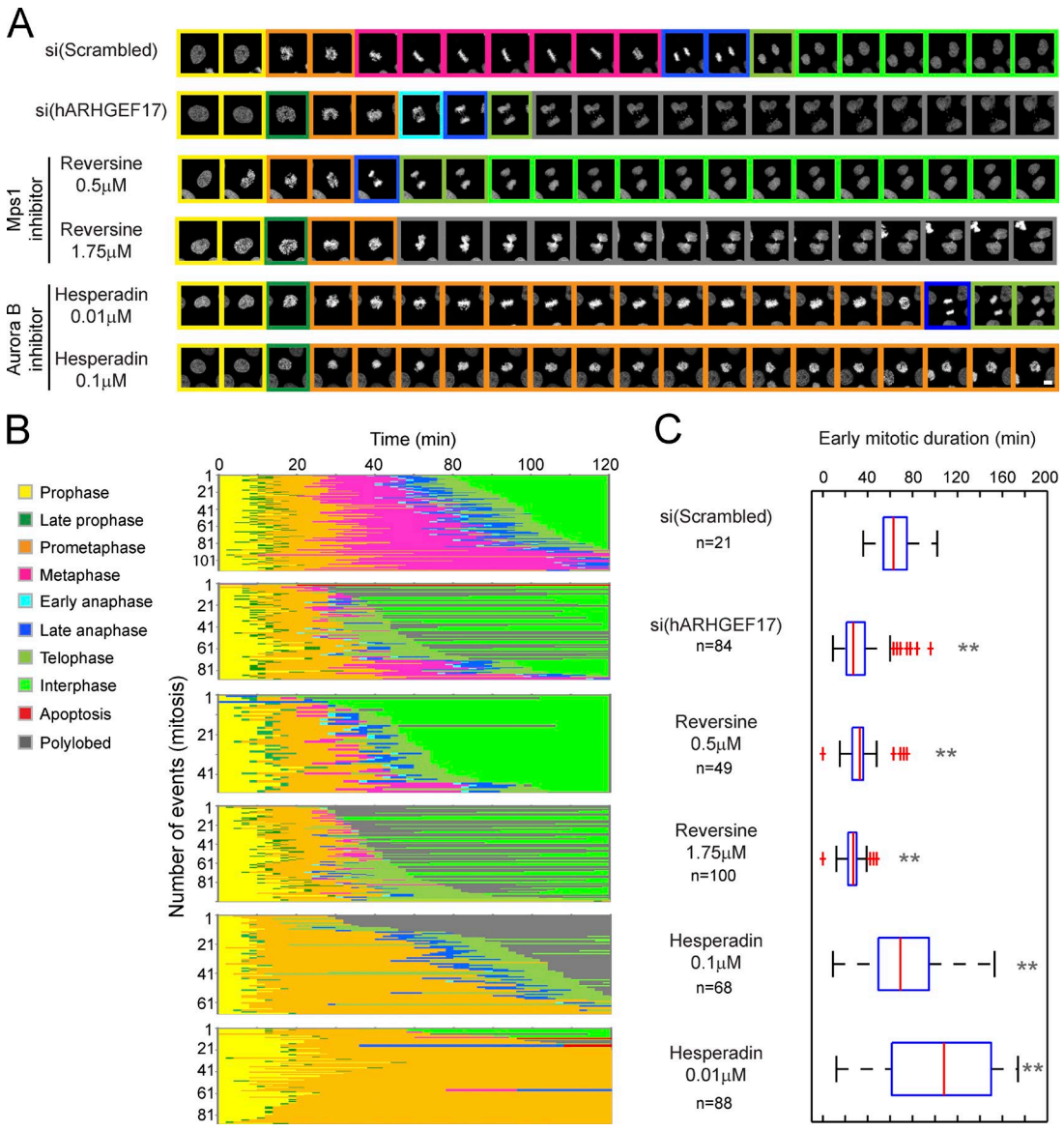

Figure 3. **ARHGEF17 knockdown phenocopies Mps1 inhibition.** Mitosis and nuclear morphology automatically extracted after si(Scrambled), si(hARHGEF17) knockdown (KD), reversine, and hesperadin treatment conditions. Colors indicate H2B-mCherry morphology classes. (A) Examples of single mitotic events. Δt is 9 min. Bar, 10 µm. (B) Automated extraction of mitotic events and morphology classes. (C) Comparison of early mitotic duration (prometa + metaphase) of >21 mitotic events (*n* indicated for each condition)/three independent experiments. Early mitotic duration in hesperadin-treated conditions was underestimated because of fixed analysis time (3 h). Boxes show median, 25–75%; whiskers show 1.5× interquartile range. **, $P < 0.01$ by two-tailed unpaired Student's *t* test compared with si(Scrambled).

to compromise SAC function in several cases (Hewitt et al., 2010; Jelluma et al., 2010; Maciejowski et al., 2010; Santaguida et al., 2010). We therefore systematically analyzed the localization of proteins representative of the different kinetochore layers and checkpoint complexes by ratiometric immunofluorescence in prometaphase cells. ARHGEF17 depletion led to a strong and significant reduction of kinetochore localization of checkpoint and outer kinetochore proteins, including Mad2, BubR1, and Bub1 (Fig. 1 G), although their overall expression level was not affected (Fig. S2, A and D). The kinetochore localization of linker and inner kinetochore proteins was affected to a lesser extent or not at all (Fig. S2 G). The strong targeting defect of all tested outer kinetochore and checkpoint proteins explains the absence of SAC activity after ARHGEF17 depletion.

The mitotic function of ARHGEF17 resides in a central domain and is independent of its Rho GEF activity

ARHGEF17's only functionally annotated domain has been shown to function as a GTP exchange factor for the small GTPase Rho in interphase (Rümenapp et al., 2002). To determine which part of hARHGEF17 is required for the SAC, we truncated hARHGEF17, introduced silent siRNA resistance mutations (Fig. 2, A and B), and tested which of the proteins could rescue the mitotic phenotype of ARHGEF17 knockdown. In contrast to hARHGEF17 containing only either the N or C terminus alone, both fragments containing the central (aa 667–1,306) domain (ΔN-mEGFP and ΔNC-mEGFP) were able to fully rescue the hARHGEF17 depletion in HeLa cells and reduced the abundance of polylobed nuclei to levels indistinguishable from

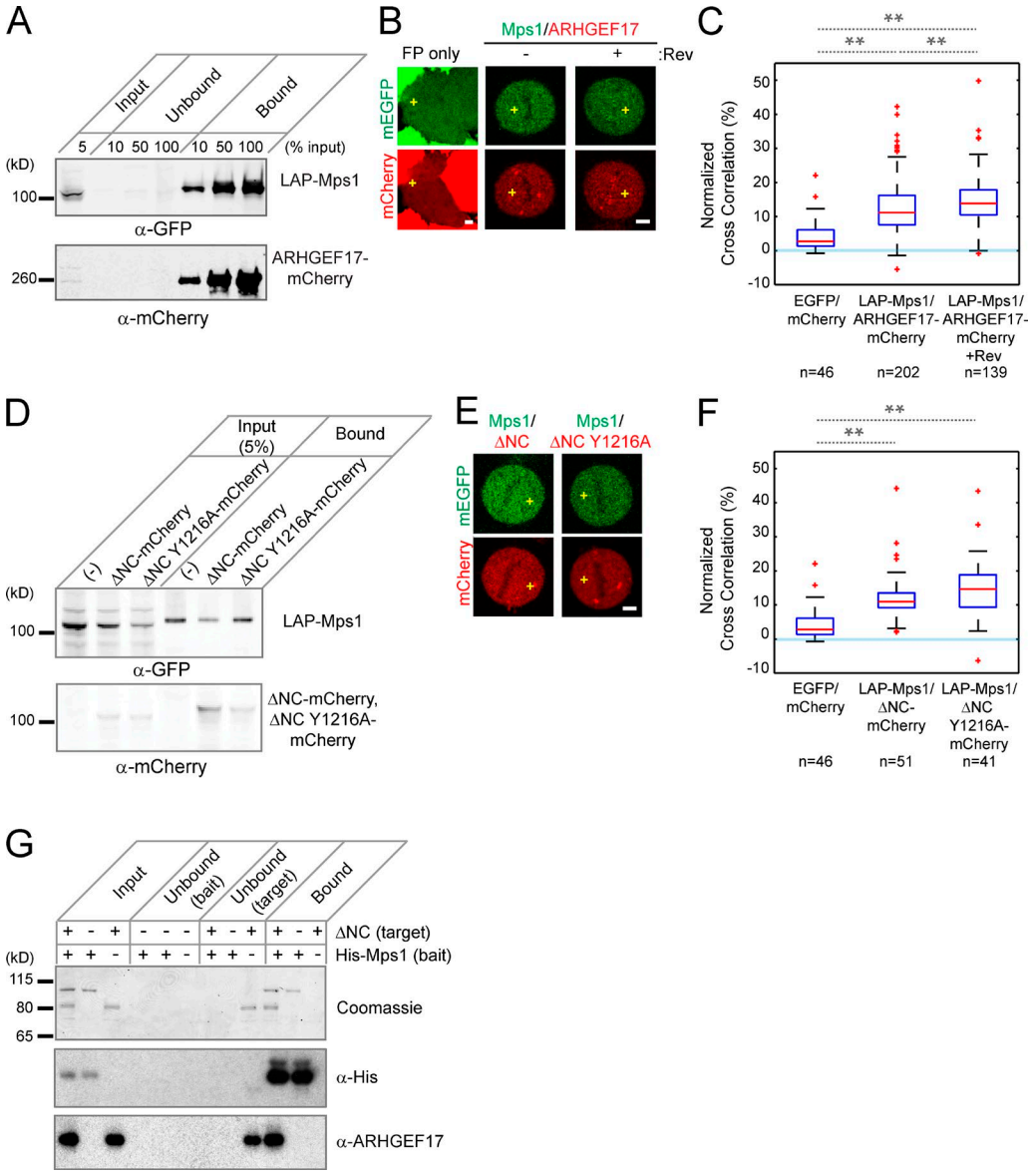

Figure 4. **ARHGEF17 and Mps1 interact during mitosis.** (A) Coimmunoprecipitation of ARHGEF17 with Mps1: LAP-tagged Mps1 (LAP-Mps1) and mCherry-tagged ARHGEF17 (ARHGEF17-mCherry) were immunoprecipitated using GFP-binding protein coupled to agarose beads. Input, supernatants (Unbound), and immunoprecipitates (Bound) were analyzed by Western Blot (anti-GFP and anti-mCherry). (B and C) FCCS of Mps1 and ARHGEF17. Exemplary cells (B; yellow crosses mark position for FCCS measurement) and normalized cross-correlation (C) of ARHGEF17-mCherry and LAP-Mps1 with or without reversine treatment of >40 cells (specific numbers indicated)/three independent experiments. (D) Coimmunoprecipitation of ARHGEF17 fragments with Mps1: LAP-Mps1 and mCherry-tagged ARHGEF17 fragments (ΔNC-mCherry and ΔNC Y1216A-mCherry) were precipitated using GFP-binding protein coupled to agarose beads. Input and precipitates were analyzed by Western blot (anti-GFP and anti-mCherry). (E and F) FCCS of Mps1 and ARH GEF17 fragments. Exemplary cells (E) and normalized cross-correlation (F) of LAP-Mps1 and ARHGEF17 fragments (ΔNC-mCherry and ΔNC Y1216A-mCherry) of >40 cells (specific numbers indicated)/three independent experiments. (G) In vitro pull-down of ARHGEF17 fragments with Mps1. His-tagged Mps1 (bait) and untagged ARHGEF17 fragments (ΔNC; target) were precipitated using His-tag binding protein coupled to Talon beads. Input, supernatants (Unbound), and precipitates (Bound) were analyzed by Western blot (anti–His-tag [middle] and anti-ARHGEF17 [bottom]). Coomassie brilliant blue staining was used as internal protein control in each condition. Boxes show median, 25–75%; whiskers show 1.5× interquartile range. **, $P < 0.01$ by two-tailed unpaired Student's *t* test, compared with mEGFP and mCherry (C and F) or between metaphase and metaphase with reversine treatment (F). Slower migration of Mps1/ARHGEF17 bands could be caused by phosphorylation (A and D). Bars, 5 µm.

controls (Figs. 2 C and S2 H). The central domain also restored the SAC-dependent nocodazole-induced prometaphase arrest to levels similar to those of controls (Fig. 2 D). Thus, the central domain of hARHGEF17 is sufficient for SAC activity.

Since this central domain contains the well-conserved Dbl homology domain essential for the GEF activity of ARHGEF17, we introduced a point mutation in the catalytic site (ΔNC Y1216A-mEGFP; Zheng, 2001; Rümenapp et al., 2002; Fig. 2 A). Overexpression of full-length hARHGEF17 (FL-mEGFP) carrying the point mutation Y1216A (FL Y1216A-mEGFP) inhibited cytokinesis, leading to an overabundance of binucleated cells, similar to the Rho inhibitor CT04, suggesting that the Y1216A mutation produced an enzymatically dead GEF that can inhibit Rho's cytokinesis activity (Fig. 2 E). In contrast, the GEF-dead central domain construct ΔNC Y1216A fully rescued the polylobed and nocodazole early-mitotic-arrest phenotypes caused by ARHGEF17 depletion (Fig. 2, C and D). The mitotic SAC function of hARH GEF17 is therefore independent of its Rho GEF activity.

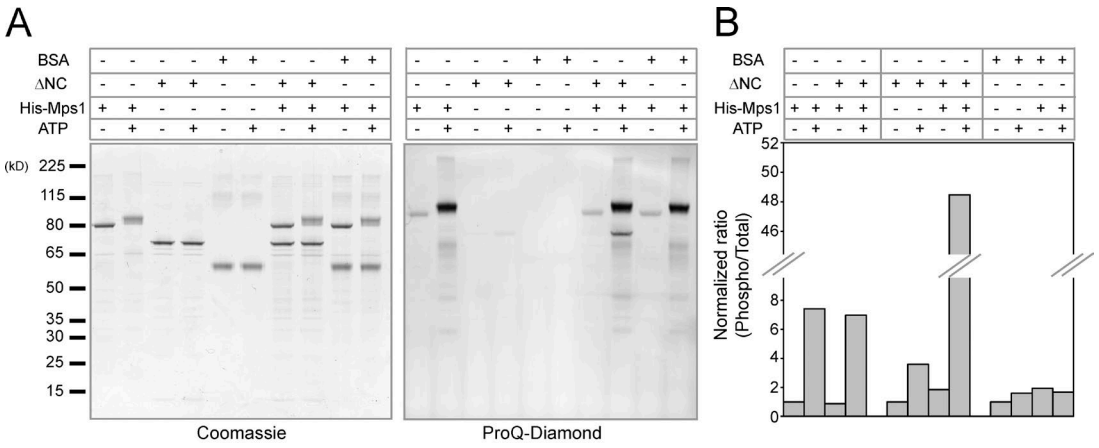

C

Residue	Sequence of best scoring peptide	Score difference	Probability	Andromeda Score
T119	AATSEEP**pT**GFSVDSN	35.72	1	150.64
T312	DEGSQDQ**pT**G**S**LSR	58.15	1	257.95
T375	AHPTLQAP**S**LEDV**pT**K	15.32	0.971	85.73

Figure 5. **Mps1 phosphorylates ARHGEF17 in vitro.** (A) In vitro kinase assay of Mps1 and ARHGEF17. Recombinant His-tag fused Mps1 (kinase) and untagged ARHGEF17-ΔNC or BSA (substrate) were incubated in the presence or absence of ATP. Total protein was visualized with Coomassie brilliant blue (CBB; left), and phosphorylated protein was visualized with Pro-Q Diamond (right). (B) Comparison of normalized mean intensity ratio between phosphorylated protein and total protein in each condition. Quantification was performed from single experiment. (C) Potential phosphorylation sites of ARHGEF17 by Mps1 identified by LC-MS/MS. Andromeda score, probability, and delta score are indicated for each site (see Materials and methods).

ARHGEF17 depletion phenocopies Mps1 inhibition

Given the strong checkpoint phenotype and loss of kinetochore protein localization, we reasoned that ARHGFEF17 could function in the regulation of SAC establishment or maintenance. Two mitotic kinases, Aurora B and Mps1, are known to be involved in the recruitment of checkpoint components to kinetochores, which are essential to establish the SAC (Lan et al., 2004; Meraldi et al., 2004; Hewitt et al., 2010; Jelluma et al., 2010; Maldonado and Kapoor, 2011; Saurin et al., 2011). To test whether ARHGEF17 acts through Mps1 or Aurora B, we compared the mitotic phenotype of ARHGEF17-depleted cells with the phenotypes of cells in which either kinase was inhibited with increasing doses of the specific small molecule inhibitors reversine or hesperadin (Hauf et al., 2003; Santaguida et al., 2010) by confocal time-lapse imaging and single-cell trajectory analysis with CellCognition (Fig. 3 A). Mps1 inhibition accelerated mitosis in a manner kinetically similar to ARH GEF17 depletion (Fig. 3 B), resulting in an indistinguishable mean early mitotic duration (Fig. 3 C). In contrast, Aurora B inhibition led to a very different phenotype of long prometaphase arrest followed by cytokinesis defects (Fig. 3, B and C). The two kinase inhibitors remained phenotypically distinct across different inhibitor concentrations. These results suggest that ARHGEF17 acts through Mps1 to ensure SAC activity.

ARHGEF17 and Mps1 interact during mitosis and Mps1 phosphorylates ARHGEF17

If ARHGEF17 acts through Mps1 in SAC regulation, interaction during mitosis is likely. To test this, we immunoprecipitated localization and affinity purification (LAP)–tagged Mps1 stably expressed from a BAC in HeLa cells that were also transfected with ARHGEF17-mCherry. Mps1 coimmunoprecipitated ARH GEF17 from mitotic cell extracts (Figs. 4 A and S3 A). To assay the interaction between Mps1 and ARHGEF17 in live mitotic cells, we performed fluorescence cross-correlation spectroscopy (FCCS; Kohl et al., 2005; Maeder et al., 2007; Huet et al., 2010; Wachsmuth et al., 2015) in the same ARHGEF17-mCherry/LAP-Mps1 coexpressing cells used for immunoprecipitation, after arresting them in metaphase with the proteasome inhibitor MG132 to prevent mitotic exit. When probing single-molecule cofluctuations of red fluorescent ARHGEF17 with green fluorescent Mps1 (Fig. 4 B), we detected a significant cross-correlation (12.4 ± 7.7%) between ARHGEF17 and Mps1, demonstrating that both proteins were moving as one particle in the cell, whereas the cross-correlation between the two fluorescent proteins alone was negligible at only 5.1 ± 5.5% (Fig. 4 C). The ARHGEF17–Mps1 interaction was specific to mitosis, as no significant cross-correlation (4.8 ± 5.5%) was observed in interphase cells (Fig. S3 C).

Having demonstrated an interaction between the full-length proteins in mitotic cells, we repeated immunoprecipitation and FCCS with the central active domain (ΔNC) of ARHGEF17, which also interacted with Mps1, independently of its Rho-GEF activity (ΔNC Y1216A) and specifically in mitosis (Fig. 4, D–F; and Fig. S3, B and C). To test whether the interaction between ARHGEF17 and Mps1 is direct, we purified recombinant ARH GEF17-ΔNC and His-tagged Mps1 from *Escherichia coli* and performed in vitro pull-down assays. ARHGEF17-ΔNC was precipitated by His-Mps1 protein bound to beads (Figs. 4 G and S3 D), but was not precipitated by His-tagged BubR1 (kinase domain) used as a negative control (Fig. S3 E). In summary, ARHGEF17 binds to Mps1 in extracts and living cells in a mitosis-specific manner, and the central domain (aa 667–1,306) is sufficient for this interaction and can interact directly with Mps1 in vitro.

Interestingly, we noticed that the Mps1 and ARHGEF17 complex in live metaphase cells is significantly enhanced by acute reversine inhibition of Mps1 (Fig. 4, B and C; and Fig. S3 C). To examine whether ARHGEF17 is an Mps1 substrate, we performed in vitro phosphorylation assays with the recombinant proteins. Indeed, ARHGEF17-ΔNC was phosphorylated

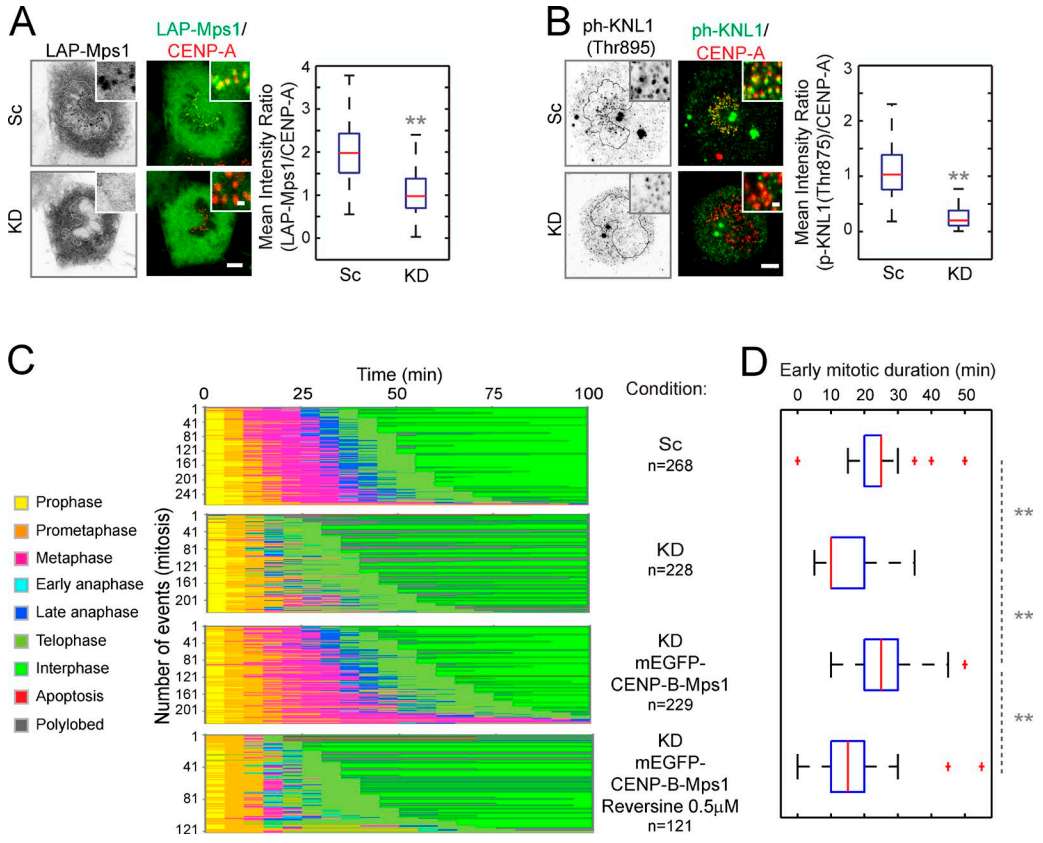

Figure 6. **ARHGEF17 is required for targeting of Mps1 at kinetochores, and constitutive tethering of Mps1 to the kinetochore replaces ARHGEF17's SAC function.** (A and B, left) Exemplary prometaphase cells with LAP-Mps1 and phospho-KNL1 labeled at kinetochores. Overlay shows LAP-Mps1 (A) or ph-KNL1 (Thr875; B; green) and CENP-A (red) after knockdown of ARHGEF17. (insets) High magnification of kinetochores. (right) Quantitative ratiometric comparison of LAP-Mps1 (A) or ph-KNL1 (B). Box plot comparing the mean intensity ratio between LAP-Mps1/CENP-A or ph-KNL1/CENP-A ratio of >600 individual sister kinetochores/three independent experiments. Bars: (main) 5 µm; (insets) 0.5 µm. (C and D) Phenotypic rescue by artificial kinetochore tethering of Mps1 in the absence of ARHGEF17. (C) Mitotic events were automatically extracted after knockdown in cells stably expressing H2B-mCherry and mEGFP-CENP-B-Mps1 with or without 0.5 µM reversine treatment. Colors indicate H2B-mCherry morphology classes. (D) Comparison of early mitotic duration. Box plot comparing the duration of prometaphase and metaphase in each condition. Mean and standard deviation of >120 mitotic events (*n* indicated for each condition)/three independent experiments. Boxes show median, 25–75%; whiskers show 1.5× interquartile range. **, $P < 0.01$ by two-tailed unpaired Student's *t* test, compared with si(Scrambled) (A and B), si(Scrambled) versus si(ARHGEF17); si(hARHGEF17) versus mEGFP-CENP-B-Mps1 expression with or without reversine (D). Sc, Scrambled; KD, knockdown.

by His-tagged Mps1 protein, whereas BSA, used as a negative control, was not a substrate (Fig. 5, A and B). Furthermore, using liquid chromatography-tandem mass spectrometry (LC-MS/MS), we identified three threonines (T119, T312, and T375) in ARHGEF17 that were phosphorylated by Mps1 (Fig. 5 C). ARHGEF17 is therefore a substrate of Mps1 kinase.

ARHGEF17 is required for targeting of Mps1 to kinetochores

A kinase binding partner and substrate could be involved in targeting and/or activation of the kinase. To test whether ARH GEF17 is required for targeting of Mps1 to kinetochores, we investigated Mps1 localization in ARHGEF17-depleted cells by quantitative ratiometric immunofluorescence. Mps1 is normally localized both at kinetochores and in the cytoplasm in prometaphase cells. After depletion of ARHGEF17, Mps1 could no longer be detected at kinetochores, leading to a significantly reduced fluorescence ratio (Fig. 6 A), even though the overall protein expression level of Mps1 was not affected (Fig. S4 A). Furthermore, the expression of ARHGEF17-ΔNC rescued the kinetochore targeting of Mps1 (Fig. S4, B and C), indicating that the central domain is sufficient not only for binding Mps1 but also for the targeting function of ARHGEF17.

To test whether loss of Mps1 accumulation affects its activity at kinetochores, we checked the phosphorylation of its kinetochore substrate KNL1 using a phospho-specific antibody (Yamagishi et al., 2012). The significantly reduced immunofluorescence ratio showed that phosphorylation of KNL1 at kinetochores was diminished after ARHGEF17 depletion (Fig. 6 B). Therefore, ARHGEF17's central domain is necessary for targeting Mps1 to kinetochores, which in turn is required for its activity toward kinetochore substrates. To conversely test if ARHGEF17 localization depends on the presence of Mps1, we knocked down Mps1 by RNAi and quantified ARHGEF17's abundance on kinetochores. ARHGEF17 localization on kinetochores was significantly increased in Mps1-depleted cells (Fig. S4 D), which had little residual Mps1 on their kinetochores (Fig. S4 E), although overall expression of ARHGEF17 did not increase (Fig. S4 A). Thus, ARH GEF17 can bind to kinetochores independently of Mps1.

Constitutive tethering of Mps1 to the kinetochore replaces ARHGEF17's SAC function

If ARHGEF17's main mitotic function is to target Mps1 to the kinetochore, constitutive tethering of Mps1 to kinetochores should make the SAC and mitosis independent of ARHGEF17.

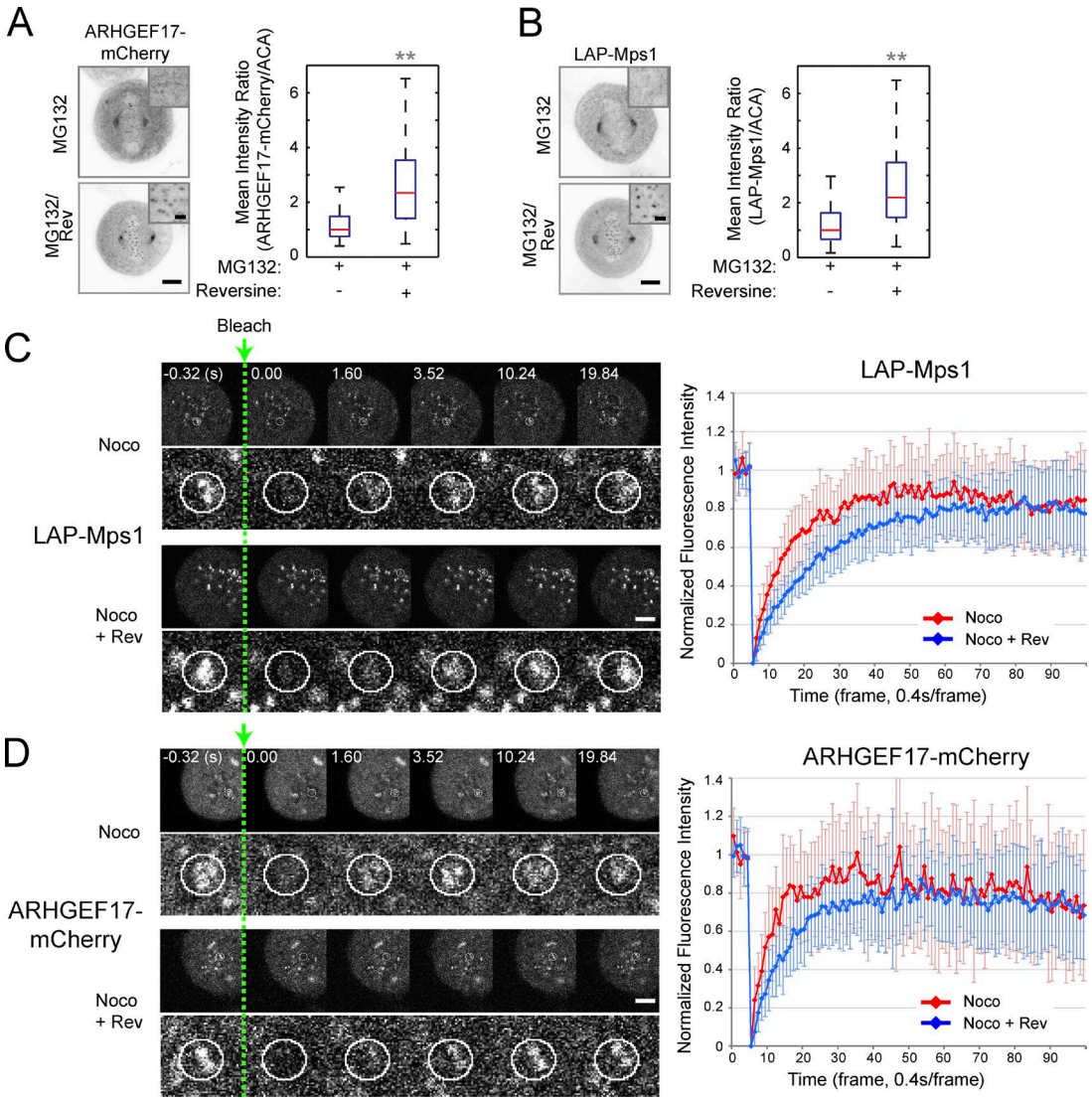

Figure 7. **ARHGEF17–Mps1 interaction is regulated by Mps1 activity.** (A and B, left) ARHGEF17 (ARHGEF17-mCherry; A) or Mps1 (LAP-Mps1; B) localization at kinetochores in prometaphase with 0.5 µM reversine (Rev; 2 h before fixation). (insets) High magnification of kinetochores. (right) Quantitative comparison of ARHGEF17-mCherry/ACA and LAP-Mps1/ACA ratios on >260 individual sister kinetochores/three independent experiments. (C and D) FRAP of Mps1 (LAP-Mps1; C) and ARHGEF17 (ARHGEF17-mCherry; D) at kinetochores in nocodazole (Noco)-treated mitotic cells with or without reversine treatment. The kinetochore region of the cell was bleached (white circles) and imaged every 0.4 s for 40 s (100 frames). (bottom) High magnification of kinetochores. FRAP curves were normalized between 1 (prebleach value) and 0 (postbleach value) and plotted over time. Boxes show median, 25–75%; whiskers show 1.5× interquartile range. **, $P < 0.01$ by two-tailed unpaired Student's *t* test compared with si(Scrambled). Bars: (A–D) 5; (A and B, insets) 1 µm.

To test this, we fused Mps1 to CENP-B, which constitutively localizes at kinetochores/centromeres, and checked whether the mitotic defects caused by ARHGEF17 depletion were rescued. In HeLa cells stably expressing CENP-B–Mps1 (at a level similar to that of endogenous Mps1; Fig. S5 A), the fusion protein localized to kinetochores throughout mitosis (Fig. S5 B), in contrast to Mps1's normally only transient kinetochore localization in prometaphase. Except for a minor delay, the presence of CENP-B–Mps1 had little effect on the division kinetics of HeLa cells (Fig. S5, C and D), which maintained normal metaphase duration, chromosome alignment, and segregation despite ARH GEF17 depletion (Fig. 6, C and D), indicative of normal SAC activity. This phenotypic rescue of ARHGEF17 knockdown by kinetochore tethering of Mps1 was dependent on its kinase activity, as it was abolished by reversine inhibition (Fig. 6, C and D) in a dose-dependent manner (Fig. S5 E). These data demonstrate that Mps1 acts downstream of ARHGEF17, whose essential mitotic function is therefore most likely the targeting of the kinase to the kinetochore.

ARHGEF17-Mps1 interaction is regulated by Mps1 activity

Our data so far favor a model in which Mps1 can be targeted to kinetochores only after binding to ARHGEF17. This complex is likely to be regulated to achieve the right concentration and activity of the kinase at the kinetochore. Because we showed that ARHGEF17 is a substrate of Mps1 (Fig. 5) and that the Mps1/ARHGEF17 interaction in the cytoplasm of live mitotic cells is enhanced upon reversine inhibition (Fig. 4, C and D), we then asked whether Mps1 activity regulates its own interaction with ARHGEF17 also at kinetochores. We first addressed this by examining whether the kinetochore

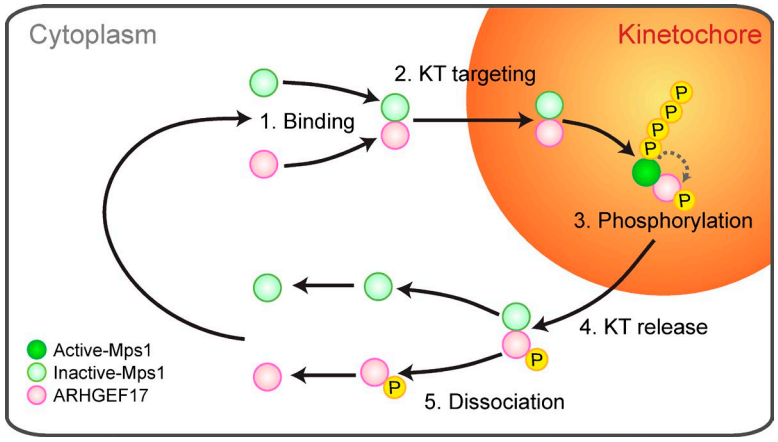

Figure 8. **Model for the recruitment of ARHGEF17 and Mps1 at kinetochores in early mitosis.** ARHGEF17 forms a complex with Mps1 in the cytoplasm, which binds to the kinetochore (KT) and allows Mps1 to phosphorylate local target substrates. Because Mps1 also phosphorylates ARHGEF17, the Mps1–ARHGEF17 complex is short lived and promotes its own dissociation, which in turn releases Mps1 and ARHGEF17 from the kinetochore. The dissociated proteins are then available to form new Mps1–ARHGEF17 complexes, presumably after dephosphorylation of ARHGEF17 by a counteracting phosphatase.

localization of Mps1 and ARHGEF17 was affected by reversine inhibition of the kinase. Indeed the localization of both interaction partners at kinetochores was significantly increased after reversine addition to MG132 metaphase-arrested cells (Fig. 7, A and B). Furthermore, FRAP assays in nocodazole-arrested prometaphase cells showed that both ARHGEF17 and Mps1 bind to kinetochores in a dynamic fashion, with half-times of a few seconds, and that the recovery of both proteins was significantly slowed down by reversine treatment (Fig. 7, C and D), whereas the recovery of Bub1 used as a control kinetochore protein was unaffected (Fig. S5 F). Collectively, these data show that kinetochore-localized ARHGEF17/Mps1 are in dynamic exchange with their cytoplasmic pool and that Mps1 activity limits its interaction with ARHGEF17 also on kinetochores.

Discussion

Model: The ARHGEF17–Mps1 complex acts as a molecular timer of Mps1 activity at the kinetochore

The molecular mechanism and regulation of the SAC are subjects of intense study. Previous studies had already shown that Mps1 plays a key role; however, how Mps1 itself is regulated is poorly understood. In this study, we characterized a newly identified essential SAC regulator, ARHGEF17. Our data demonstrate that ARHGEF17 is a binding partner and substrate of Mps1. This interaction is essential to target Mps1 kinase activity to kinetochores, which is critical for integrity of the outer kinetochore and the assembly and function of checkpoint complexes. Collectively, this provides the mechanistic explanation for ARHGEF17's novel mitotic phenotype, which is independent from its interphase function as a RhoGEF in regulation of the actin cytoskeleton. It has been reported that Ndc80 and Aurora B are needed for Mps1 localization to the kinetochores (Martin-Lluesma et al., 2002; Santaguida et al., 2011; Martin-Lluesma et al., 2002; Saurin et al., 2011; Santaguida et al., 2011; Nijenhuis et al., 2013; Zhu et al., 2013; Hiruma et al., 2015). Our data show that kinetochore localization of neither Ndc80 nor Aurora B is affected by ARHGEF17 depletion, arguing that ARHGEF17 acts directly on Mps1.

The observation that the Mps1–ARHGEF17 interaction, their kinetochore targeting, and their residence time at the kinetochore are counteracted by Mps1's activity led us to propose a model in which the Mps1–ARHGEF17 complex would act as a molecular timer of a diffusion reaction–targeting mechanism that ensures the right amount of this key mitotic kinase at kinetochores (Fig. 8). In this model, ARHGEF17 forms a complex with Mps1 in the cytoplasm. This complex can then bind to the kinetochore and allows Mps1 to phosphorylate local target substrates. Because Mps1 also phosphorylates ARHGEF17, the Mps1–ARHGEF17 complex is short lived and promotes its own dissociation, which in turn releases Mps1 and ARHGEF17 from the kinetochore. The dissociated proteins are then available to form new Mps1–ARHGEF17 complexes, presumably after dephosphorylation of ARHGEF17 by a counteracting phosphatase. It will be very interesting to further dissect the interdependence of ARHGEF17 and Mps1 function with kinase-dead Mps1–expressing cell lines in future experiments.

Although we do not have direct evidence, it is tempting to speculate that ARHGEF17 binding does not just confer kinetochore targeting to Mps1, but also activates its enzyme activity. That ARHGEF17 can localize to kinetochores even if Mps1 is knocked down suggests that Mps1 may bind ARHGEF17 both in cytoplasm and at the kinetochore. The fact that kinetochore-localized ARHGEF17 and Mps1 exchanged dynamically with the cytoplasm and resided longer at kinetochores when Mps1 was inhibited is consistent with the idea that the ARHGEF17–Mps1 complex may dissociate from the kinetochore as a unit; however, we cannot formally rule out that ARHGEF17 and Mps1 dissociate from kinetochores independently. The molecular timer mechanism we propose here, however, would work very similarly in either scenario. Such a molecular timer mechanism would be conceptually similar to the regulatory mechanism of GTPases or the ones proposed for the APC/C inhibitor Emi1 or cytosolic Mad2/Bub1 complex (Reimann et al., 2001; Maldonado and Kapoor, 2011).

Materials and methods

BAC cloning

Mouse ARHGEF17 BAC clone RP23-452C8 was obtained from BACPAC Resources. Subsequent cloning steps were performed as previously described (Poser et al., 2008). Primers for addition of the LAP tag at the C terminus were designed using the MitoCheck BACfinder resources website (http://www.mitocheck.org/cgi-bin/BACfinder): 5′-AGACCGTGGGCCGAGATGACAGCACAAACCACCTACTCCTGTGGAGGGTGGATTATGATATTCCAACTACTG-3′ and 5′-GAAGAACTGCTCAAGAAGACTCGGACGGGAGACACCGGGTCCTGAGTGGACAGGTGGACGGGAGTCGGACG-3′.

Cell lines

HeLa Kyoto cells were grown in DMEM containing 10% FBS, 2 mM glutamine, 1 mM sodium pyruvate, and 100 µg/ml penicillin and streptomycin. H2B-mCherry HeLa Kyoto cells were described previously (Neumann et al., 2010). The HeLa Kyoto cell line expressing H2B-mCherry and EGFP-LaminA was provided by the Mattaj Laboratory (European Molecular Biology Laboratory, Heidelberg, Germany). The HeLa Kyoto cell lines expressing LAP-tagged mSpc24 BAC/H2B-mCherry, LAP-tagged mZW10 BAC/H2B-mCherry, LAP-tagged hBub1, and LAP-tagged mMad2 BAC were provided by A.A. Hyman (Max Planck Institute of Molecular Cell Biology and Genetics, Dresden, Germany). H2B-mCherry was transfected into HeLa cells expressing LAP-tagged mMad2 BAC with Fugene6 (Promega) according to the manufacturer's instructions. A clone stably expressing H2B-mCherry was isolated by selection with 0.5 µg/ml puromycin (Calbiochem). LAP-tagged mouse ARHGEF17 BAC was transfected into HeLa cells expressing H2B-mCherry with Lipofectamine 2000 (Invitrogen) according to the manufacturer's instructions. A clone stably expressing LAP-tagged mARH GEF17 BAC was isolated by selection with 500 µg/ml Geneticin (Invitrogen). The HeLa Kyoto cell line expressing LAP-tagged hMps1 BAC was provided by A. Mussachio (Max Planck Institute of Molecular Biology, Dortmund, Germany). The ARHGEF17 fragment (ARHGEF17 [667–2,063]-mEGFP: ΔN, ARHGEF17 [667–1,306]-mEGFP: ΔNC, ARH GEF17 [667–1,306]–Y1216A-mEGFP: ΔNC Y2116A, ARHGEF17 [1–582]-mEGFP: ΔC-siRa [mutations: C1502T, A1508C, and G1511A], ARHGEF17 [109–664]-mEGFP: ΔC-siRb [mutations: C1508C, G1511A, T1514C, and G1517A], ARHGEF17 [1,304–2,063]-mEGFP: ΔN1, or mEGFP-ARHGEF17 [1,304–2,063]: ΔN2) or mEGFP-CEN PB-Mps1 was transfected into HeLa cells expressing H2B-mCherry with Fugene6 (Promega) according to the manufacturer's instructions. A clone stably expressing each ARHGEF17 fragment or mEGFP-CEN PB-Mps1 was isolated by selection with 500 µg/ml Geneticin.

RNA interference

siRNAs (Ambion) are listed in Table S1.

For quantitative phenotypic time-lapse imaging, cells were seeded on ready-to-transfect 8-well LabTEK slides (Thermo Fisher Scientific) as described previously (Erfle et al., 2008; Neumann et al., 2010). For quantitative immunofluorescence, siRNA was transfected using Lipofectamine 2000.

High-resolution time-lapse microscopy imaging

Images were acquired with the LAS AF and Matrix Screen Application software on an SP5 confocal microscope with a 63× PlanApochromat oil objective, NA 1.4 (Leica). Live-cell imaging was performed at 37°C using CO_2-independent medium without phenol red (Custom StemSpan SFEM by Stem Cell) containing 20% FBS, 2 mM L-glutamine, and 100 mg/ml penicillin and streptomycin. Images were acquired every 3 min.

Automatic quantitative phenotypic time-lapse imaging and analysis

To quantify the occurrence of the mitotic phenotypes, images were acquired with CellR software on an automated ScanR epifluorescence microscope (Olympus) with Plan 10×, NA 0.4 air objective (Olympus), and analyzed as described previously (Held et al., 2010; Neumann et al., 2010; Walter et al., 2010). To quantify the duration of prometaphase and metaphase, images were acquired with ZEN 2010 software on a confocal microscope (LSM 780; ZEISS) with a 63× PlanApochromat oil objective, NA 1.4 (ZEISS). Live-cell imaging was performed at 37°C using CO_2-independent medium without phenol red (Custom StemSpan SFEM) containing 20% FBS, 2 mM L-glutamine, and 100 mg/ml penicillin and streptomycin. Automated quantitative analysis of dividing H2B-mCherry–expressing cells was used to monitor mitotic progression in single cells. For this, nuclei were detected in the H2B-mCherry channel and classified as previously described (Held et al., 2010; Walter et al., 2010). For classification of nuclei in images acquired every 5 min (Figs. 6 and S5), we defined nine morphological classes: interphase, prophase, prometaphase, metaphase, early anaphase, late anaphase, telophase, cell death, and polylobed nuclei. For experiments with image acquisition every 3 min (Fig. 3), the prophase class was split into two classes corresponding to early and late prophase. The training set contained ∼1,000 manually labeled nuclei, which were detected with an overall accuracy of >90.0% in 10-fold cross-validation. Cells were tracked with a constrained nearest-neighbor tracking procedure, and mitotic onset was detected as interphase–prophase or interphase–prometaphase transition. To reduce the effect of classification errors on phase length measurements, classification results were corrected with hidden Markov models (Held et al., 2010; Walter et al., 2010). To inhibit the Rho activity of hARHGEF17, CT04 (Cytoskeleton) was treated before imaging, and cells were then imaged for 24 h (Fig. 2 E).

Immunofluorescence

All steps were performed at RT. Cells were fixed with 3.7% paraformaldehyde in PHEM buffer (45 mM Pipes, 45 mM HEPES, 10 mM EGTA, 5 mM $MgCl_2$, and 1 mM PMSF, pH 6.8) for 10 min and permeabilized for 10 min with 0.2% Triton X-100 in PHEM buffer. Cells were blocked with 2% BSA in PHEM buffer for 1 h. Samples were incubated with primary antibodies in 2% BSA in PHEM buffer for 2 h, washed, and incubated with secondary antibodies for 60 min in 2% BSA in PHEM. After washing, they were imaged in PHEM buffer with ZEN 2010 software on a confocal microscope with a 63× PlanApochromat oil-objective, NA 1.4 (ZEISS). The following antibodies were used: anti-hARHGEF17 (rabbit; Abcam) 1:100 and anti-CREST (anti-centromere antibody [ACA], human; Europe Bioproducts) 1:500. Secondary antibodies were anti–rabbit Alexa Fluor 488 (Molecular Probes) 1:500 and anti–human Alexa Fluor 647 (Molecular Probes) 1:500. DNA was stained with Hoechst 33342 (Sigma-Aldrich). To retrieve the antigen of hARHGEF17 in HeLa Kyoto cells, cells were incubated with 1% SDS (SERVA) for 5 min after cells were fixed with 3.7% paraformaldehyde in PHEM buffer (Fig. S2 E).

Quantitative immunofluorescence at kinetochore

Immunofluorescence and imaging were performed as described earlier. The following antibodies were used: anti-GFP (rabbit, MBL) 1:500, anti-CENPA (mouse, 3-19; MBL) 1:100, anti-Mad2 (mouse, COV ANCE) 1:100, anti-Bub1 (mouse, 14H5; Millipore) 1:100, anti-BubR1 (mouse, 8G1; MBL) 1:100, anti-CREST (ACA, human) 1:500, anti-BLINKIN, and anti-ZW10 (mouse, gift from J. Swedlow, Dundee University, Dundee, Scotland, UK) 1:50, and anti–ph-KNL1 (Thr875; rabbit; gift from Y. Watanabe, Tokyo University, Tokyo, Japan; Yamagishi et al., 2012) 1:2,000. Secondary antibodies were anti–mouse Alexa Fluor 488 (Molecular Probes) 1:500, anti–rabbit Alexa Fluor 488 (Molecular Probes) 1:500, anti–mouse Alexa Fluor 546 (Molecular Probes) 1:500, and anti–human Alexa Fluor 647 (Molecular Probes) 1:1,000. To measure target protein expression levels at kinetochores/centromeres in 3D images, segmentation of the mCherry or Hoechst 33342 channel was used to create a chromosome mask within which anti–CENP-A spots were detected where the mean intensities of anti–CENP-A or ACA marker protein were measured. To correct for variability in the intensity of the target kinetochore proteins, we normalized the target signal to the kinetochore signal of the CENP-A antibody or ACA antibody. Segmentation and intensity measurements were performed automatically by an routine developed in-house and implemented in Fiji (https://github.com/cmci/3D-DotDetection; Sbalzarini and Koumoutsakos, 2005; Schindelin et al., 2012).

Mitotic chromosome spreads

HeLa Kyoto cells were cultured for 21 h in the presence of 0.33 µM nocodazole (Sigma-Aldrich). Cells arrested in mitosis were then harvested by shake-off, treated with a hypotonic buffer (16.6% FBS in sterilized water) for 5 min at 37°C, and attached to micro–cover glass (Deckglaser; Carolina Biologicals) with a Cytospin 4 Centrifuge (Thermo Fisher Scientific). The cells on the glass slide were fixed with the paraformaldehyde solution described earlier, followed by immunofluorescence.

Western blotting

Cells were resuspended in ice-cold lysis buffer (10 mM Tris-Cl, pH 7.5, 150 mM NaCl, 0.1% SDS, 5 mM EDTA, and 1% Triton X-100) supplemented with complete protease inhibitor cocktail and PhosSTOP phosphatase inhibitor cocktail (Roche). After 30-min incubation on ice, cells were centrifuged and the supernatants were collected. Cell lysates were loaded into NuPAGE 4–12% Bis-Tris Mini Gels (Life Technologies) and transferred to PVDF membranes (Millipore). The following antibodies were used for Western blotting: anti-ARHGEF17 (rabbit, ab67278; Abcam) 1:1,000, anti-GFP (mouse, 7.1/3.1; Boehringer Mannheim; and rabbit; MBL) 1:1,000, anti-Aurora B (mouse, 6; BD Transduction; and rabbit; Abcam) 1:1,000, anti-GAPDH (mouse, 6C5; Santa Cruz Biotechnology) 1:2,000, anti-Mad2 (mouse; COVANCE) 1:500, anti-Bub1 (mouse, 14H5; Millipore) 1:1,000, anti-BubR1 (mouse, 8G1; MBL) 1:1,000, anti-Mps1 (sheep, gift from S.S. Taylor, Manchester University, Manchester, England, UK; Tighe et al., 2008) 1:2,000, anti-DsRed/mCherry (rabbit; Clontech) 1:1,000, and anti-His (mouse; Qiagen) 1:2,000. Secondary antibodies were anti–mouse Alexa Fluor 680 (Molecular Probes) 1:15,000, anti–rabbit Alexa Fluor 680 (Molecular probes) 1:15,000, anti-mouse IRDye800CW (LI-COR Biosciences) 1:10,000, anti-rabbit IRDye800CW (LI-COR Biosciences) 1:10,000, anti-sheep IRDye800CW (LI-COR Biosciences) 1:10,000, HRP-conjugated anti-mouse (Promega) 1:5,000, and HRP-conjugated anti-rabbit (Promega) 1:5,000. Blots were scanned using the Odyssey imaging device (LI-COR Biosciences) or detected with ECL (GE Healthcare).

Immunoprecipitation

Cells were resuspended in ice-cold lysis buffer (10 mM Tris-Cl, pH 7.5, 150 mM NaCl, 0.1% SDS, 1% Triton X-100, 1% deoxycholate, and 5 mM EDTA, supplemented with complete protease inhibitor cocktail, PhosSTOP phosphatase inhibitor cocktail [Roche], Benzonase [Sigma-Aldrich], and 1 mM PMSF). After incubation for 30 min on ice, cells were centrifuged, and the supernatants were collected. Agarose beads coupled to GFP-binding protein (GFP-Trap_A; Chromotek) were prewashed, added to the supernatants, and incubated for 1 h at 4°C. The beads were then washed three times with lysis buffer and resuspended in SDS-PAGE sample buffer.

FCCS

Measurements and analysis were performed as previously described (Wachsmuth et al., 2015), using a ConfoCor3 system (LSM 780; ZEI SS). In brief, light was focused by a water immersion 40× 1.2-NA objective and collected by two avalanche photodiodes in the spectrally distinct regions 505–540 nm (F_g) and 600–650 nm (F_r) after passing through a pinhole set to 1 Airy unit. Samples were incubated at 37°C and excited with 488- and 561-nm lasers, using minimal power (<1 kW · cm^{-2}) to reduce photobleaching, photophysical effects, and cellular toxicity. The instrument was calibrated using Alexa Fluor 488 and 568 to align the pinholes, perform cover glass corrections, and determine the size and geometry of the focal volume before each experiment. Each measurement was taken for 45 s in total, with cells selected manually based on relatively low expression levels below an arbitrary threshold count rate of 1,000 kHz. For measurements of transiently transfected ARHGEF17-mCherry and EGFP-MPS1 stably expressed from a BAC, count rates in the mCherry channel were consistently higher relative to the GFP channel, as were counts per molecule (mean count rate/particle number), therefore minimizing spectral cross-talk (Bacia et al., 2012). Cross-talk was quantified using mEGFP expressed alone, and an EGFP-MBP-mCherry fusion protein was used as a positive control of the maximum measurable cross-correlation in our setup. Measurements in transfected control cells were taken 24 h after transfection. For experiments including reversine, 0.5 µM reversine was added 0.5 h before imaging to cells synchronized in metaphase by prior treatment with 20 µM MG132.

Data analysis was performed in Fluctuation Analyzer software as previously described (Wachsmuth et al., 2015). Calculation of photobleaching-corrected correlation functions was followed by corrections for photobleaching, background, spectral cross-talk, nonperfect overlap of the observation volumes, and fluorophore maturation (Boeke et al., 2014) and complemented by fitting the data with model functions for 3D normal/anomalous diffusion, resulting in normalized cross-correlation amplitudes between ∼0 for the negative and ∼0.5 for the positive control.

FRAP

FRAP experiments were performed on a confocal microscope with a water immersion 40× NA 1.2 objective. HeLa Kyoto cells stably expressing Mps1 fused with LAP, ARHGEF17 fused with mCherry, or Bub1 fused with LAP were imaged. Five prebleach images were acquired before bleaching. The signal at the kinetochore in nocodazole mitotic-arrested cells was then photobleached in nine iterations with full intensity of the 488- or 561-nm lasers. Fluorescence recovery was followed every 0.4 s for a total time of 40 s. Intensity values were normalized between 1 (prebleach) and 0 (postbleach) after subtraction of acquisition bleaching and background. The $t_{1/2}$ value was defined as the half-maximal recovery time of the mobile fraction of each condition.

Purification of ARHGEF17 recombinant protein

The human ARHGEF17 fragment (aa 667–1,306; ΔNC) was cloned into a pFastBac-HT vector (pFastBac-HT-ΔNC; Invitrogen) and expressed using the baculovirus protein expression system. Pellets from 1 liter of infected Sf21 cells were resuspended in buffer (50 mM Tris-HCl, pH 7.5, 500 mM NaCl, 5 mM $MgCl_2$, 250 mM sucrose, 1 mM DTT, 10 mM imidazole, SmDNase, and complete protease inhibitor), lysed by sonication, and centrifuged for 30 min at 4°C, 30,000 *g*. The supernatant was collected and incubated with 2 ml NiNTA Agarose resin for 30 min at RT. Beads were collected and washed with buffer, and the protein was eluted with elution buffer (50 mM Tris-HCl, pH 7.5, 500 mM NaCl, 5 mM $MgCl_2$, 250 mM sucrose, 1 mM DTT, and 250 mM imidazole). The eluted fractions were pooled and dialyzed into ion exchange chromatography (IEX) running buffer (50 mM Tris-HCl, pH 7.5, 50 mM NaCl, and 1 mM DTT) overnight at 4°C, purified using a HiTrapQ column, and eluted with a gradient IEX elution buffer (50 mM Tris-HCl, pH 7.5, 1 M NaCl, and 1 mM DTT). Eluted fractions were then dialyzed into 25 mM Tris, pH 7.6, 150 mM NaCl, 1 mM TCEP, 0.2% Triton X-100, and 5% glycerol and concentrated.

For the kinase assay and mass spectroscopy, part of the pooled and eluted fractions after the initial NiNTA purification were dialyzed into phosphatase buffer (50 mM Hepes, pH 7.5, 50 mM NaCl, 2 mM DTT, and 0.01% Brij35) and treated with Lambda phosphatase (New England Biolabs, Inc.) for 1 h at 30°C. The sample was adjusted to 250 mM NaCl and 10 mM imidazole and incubated with NiNTA as described earlier to remove the phosphatase. It was then further purified by IEX as described earlier. The His-tag was optionally removed by incubation with TEV protease for further experiments.

In vitro pull-down assay

Pull-downs were performed with 1 µg of each recombinant protein in an equilibration buffer containing 25 mM Tris-HCl, pH 7.6, 150 mM NaCl, 5% glycerol, and 0.1% Triton X-100. Either His-tagged Mps1 alone or His-tagged BubR1 (kinase domain) was used as affinity bait on the TALON Metal Affinity Resin (Clontech) for 1 h at 4°C. The washed beads were then incubated with nontagged ARHGEF17 (aa 667–1,306) for 1 h at 4°C. After washing with the equilibration buffer, the beads were analyzed for protein content by SDS-PAGE. His-tagged Mps1 and BubR1 recombinant protein were provided by A. Mussachio.

In vitro kinase assay

200 nM of Mps1 and ARHGEF17 or BSA with 200 nM of each were incubated with kinase buffer containing 12.5 mM Tris-Cl, pH 7.5, 35 mM KCl, 1 mM $MgCl_2$, 50 µM EGTA, 100 µM DTT, and 1× phosStop (Roche) at 30°C for 3 h in the absence or presence of ATP/Mg cocktail (0.25 mM ATP; Merck). The reaction was stopped with 20 mM EDTA. The samples were separated by SDS-PAGE gel and stained with colloidal Coomassie (Sigma-Aldrich), or they were blotted and the phosphorylated protein was visualized with Pro-Q Diamond (Life Technologies) and visualized using the Typhoon imaging device (Fuji).

LC-MS/MS

Samples were separated by SDS-PAGE and stained with Coomassie. The bands were cut from the gel digested with trypsin, and the peptides were extracted. Peptides were separated using the Waters nanoAcquity UPLC system. After the peptides were trapped with the column, the outlet of the analytical column was coupled directly to the mass spectrometer (Orbitrap Velos Pro; Thermo Fisher Scientific). The most intense ions (up to intensity 15) from the full-scan MS were selected for sequencing. After processing the data using MSConvert (ProteoWizard, v.2.0) and Mascot (v2.2.07), with which the data were searched against a Uniprot human database with a list of common contaminants appended, to ascertain the protein identifications of the gel bands, the data were searched with MaxQuant (v1.2.2.5) against a database containing the sequences of the identified proteins. The data were searched with the following modifications: carbamidomethyl (C; fixed) AND phospho (STY) AND oxidation (M; variable). Only phosphopeptides with Andromeda score >60 were reported, and only the phosphorylation sites with a probability score higher than 0.75 and a score difference (delta score) higher than 5 were considered (Marchini et al., 2011).

Online supplemental material

Table S1 shows the list of siRNAs. Fig. S1 shows knockdown efficiency and rescue validation for ARHGEF17. Fig. S2 demonstrates specificity of ARHGEF17 knockdown, endogenous ARHGEF17 localization, effect on additional kinetochore protein targeting by ARH GEF17 knockdown, and ARHGEF17 fragment rescue controls. Fig. S3 shows that ARHGEF17 and Mps1 interact during mitosis. Fig. S4 demonstrates that ARHGEF17 is essential for kinetochore targeting of Mps1. Fig. S5 shows that constitutive localization of Mps1 rescued the effect of ARHGEF17 knockdown during mitosis and FRAP data of a control kinetochore protein. Online supplemental material is available at http://www.jcb.org/cgi/content/full/jcb.201408089/DC1.

Acknowledgments

We thank Andrea Musacchio, Claudia Breit, Ina Poser, Anthony A. Hyman, Yoshinori Watanabe, Jason Swedlow, Moritz Mall, and Stephen S. Taylor for providing materials; Malte Wachsmuth (European Molecular Biology Laboratory [EMBL]) for help with FCCS; and all the members of the EMBL Advanced Light Microscopy Facility for technical support in image acquisition and analysis. EMBL's protein expression core facility is acknowledged for help in producing recombinant ARHGEF17 and EMBL's proteomics core facility for LC-MS/MS assay and data analysis. The Dortmund Protein Facility is acknowledged for the production of recombinant Mps1 and BubRI.

This study was supported by the European Commission within the EU-FP7-MitoSys consortia and EU-FP7-Systems Microscopy NoE (grant agreements 241548 and 258068 to J. Ellenberg), the Alexander von Humboldt-Stiftung (7000247787 to M. Isokane), the Wellcome Trust Henry Wellcome Fellowship (100090/Z/12/Z to R. Mahen), the Cluster of Excellence Cell Networks (EXC 81 to R. Mahen), European Molecular Biology Organization long-term fellowships (ALTF 416-2012 and GA-2010-2767146 to R. Mahen), Human Frontier Science Program long-term fellowship (LT00215/2007-L to T.S. Kitajima), and the European Molecular Biology Laboratory (M. Isokane, T. Walter, R. Mahen, B. Nijmeijer, J.K. Hériché, K. Miura, T.S. Kitajima, and J. Ellenberg).

The authors declare no further competing financial interests.

Submitted: 21 August 2014
Accepted: 11 February 2016

References

Abrieu, A., L. Magnaghi-Jaulin, J.A. Kahana, M. Peter, A. Castro, S. Vigneron, T. Lorca, D.W. Cleveland, and J.-C. Labbé. 2001. Mps1 is a kinetochore-associated kinase essential for the vertebrate mitotic checkpoint. *Cell.* 106:83–93. http://dx.doi.org/10.1016/S0092-8674(01)00410-X

Alexandru, G., W. Zachariae, A. Schleiffer, and K. Nasmyth. 1999. Sister chromatid separation and chromosome re-duplication are regulated by different mechanisms in response to spindle damage. *EMBO J.* 18:2707–2721. http://dx.doi.org/10.1093/emboj/18.10.2707

Bacia, K., Z. Petrášek, and P. Schwille. 2012. Correcting for spectral cross-talk in dual-color fluorescence cross-correlation spectroscopy. *ChemPhysChem.* 13:1221–1231. http://dx.doi.org/10.1002/cphc.201100801

Boeke, D., S. Trautmann, M. Meurer, M. Wachsmuth, C. Godlee, M. Knop, and M. Kaksonen. 2014. Quantification of cytosolic interactions identifies Ede1 oligomers as key organizers of endocytosis. *Mol. Syst. Biol.* 10:756. http://dx.doi.org/10.15252/msb.20145422

Erfle, H., B. Neumann, P. Rogers, J. Bulkescher, J. Ellenberg, and R. Pepperkok. 2008. Work flow for multiplexing siRNA assays by solid-phase reverse transfection in multiwell plates. *J. Biomol. Screen.* 13:575–580. http://dx.doi.org/10.1177/1087057108320133

Foley, E.A., and T.M. Kapoor. 2013. Microtubule attachment and spindle assembly checkpoint signalling at the kinetochore. *Nat. Rev. Mol. Cell Biol.* 14:25–37. http://dx.doi.org/10.1038/nrm3494

Hardwick, K.G., E. Weiss, F.C. Luca, M. Winey, and A.W. Murray. 1996. Activation of the budding yeast spindle assembly checkpoint without mitotic spindle disruption. *Science.* 273:953–956. http://dx.doi.org/10.1126/science.273.5277.953

Hauf, S., R.W. Cole, S. LaTerra, C. Zimmer, G. Schnapp, R. Walter, A. Heckel, J. van Meel, C.L. Rieder, and J.-M. Peters. 2003. The small molecule Hesperadin reveals a role for Aurora B in correcting kinetochore-microtubule attachment and in maintaining the spindle assembly checkpoint. *J. Cell Biol.* 161:281–294. http://dx.doi.org/10.1083/jcb.200208092

He, X., M.H. Jones, M. Winey, and S. Sazer. 1998. Mph1, a member of the Mps1-like family of dual specificity protein kinases, is required for the spindle checkpoint in *S. pombe*. *J. Cell Sci.* 111:1635–1647.

Held, M., M.H.A. Schmitz, B. Fischer, T. Walter, B. Neumann, M.H. Olma, M. Peter, J. Ellenberg, and D.W. Gerlich. 2010. CellCognition: time-resolved phenotype annotation in high-throughput live cell imaging. *Nat. Methods.* 7:747–754. http://dx.doi.org/10.1038/nmeth.1486

Hewitt, L., A. Tighe, S. Santaguida, A.M. White, C.D. Jones, A. Musacchio, S. Green, and S.S. Taylor. 2010. Sustained Mps1 activity is required in mitosis to recruit O-Mad2 to the Mad1-C-Mad2 core complex. *J. Cell Biol.* 190:25–34. http://dx.doi.org/10.1083/jcb.201002133

Hiruma, Y., C. Sacristan, S.T. Pachis, A. Adamopoulos, T. Kuijt, M. Ubbink, E. von Castelmur, A. Perrakis, and G.J.P.L. Kops. 2015. CELL DIVISION CYCLE. Competition between MPS1 and microtubules at kinetochores regulates spindle checkpoint signaling. *Science.* 348:1264–1267. http://dx.doi.org/10.1126/science.aaa4055

Howell, B.J., B. Moree, E.M. Farrar, S. Stewart, G. Fang, and E.D. Salmon. 2004. Spindle checkpoint protein dynamics at kinetochores in living cells. *Curr. Biol.* 14:953–964. http://dx.doi.org/10.1016/j.cub.2004.05.053

Hübner, N.C., L.H. Wang, M. Kaulich, P. Descombes, I. Poser, and E.A. Nigg. 2010. Re-examination of siRNA specificity questions role of PICH and Tao1 in the spindle checkpoint and identifies Mad2 as a sensitive target for small RNAs. *Chromosoma.* 119:149–165. http://dx.doi.org/10.1007/s00412-009-0244-2

Huet, S., S.V. Avilov, L. Ferbitz, N. Daigle, S. Cusack, and J. Ellenberg. 2010. Nuclear import and assembly of influenza A virus RNA polymerase studied in live cells by fluorescence cross-correlation spectroscopy. *J. Virol.* 84:1254–1264. http://dx.doi.org/10.1128/JVI.01533-09

Jelluma, N., A.B. Brenkman, N.J.F. van den Broek, C.W.A. Cruijsen, M.H.J. van Osch, S.M.A. Lens, R.H. Medema, and G.J.P.L. Kops. 2008a. Mps1 phosphorylates Borealin to control Aurora B activity and chromosome alignment. *Cell.* 132:233–246. http://dx.doi.org/10.1016/j.cell.2007.11.046

Jelluma, N., A.B. Brenkman, I. McLeod, J.R. Yates III, D.W. Cleveland, R.H. Medema, and G.J.P.L. Kops. 2008b. Chromosomal instability by inefficient Mps1 auto-activation due to a weakened mitotic checkpoint and lagging chromosomes. *PLoS One.* 3:e2415. http://dx.doi.org/10.1371/journal.pone.0002415

Jelluma, N., T.B. Dansen, T. Sliedrecht, N.P. Kwiatkowski, and G.J.P.L. Kops. 2010. Release of Mps1 from kinetochores is crucial for timely anaphase onset. *J. Cell Biol.* 191:281–290. http://dx.doi.org/10.1083/jcb.201003038

Kang, J., Y. Chen, Y. Zhao, and H. Yu. 2007. Autophosphorylation-dependent activation of human Mps1 is required for the spindle checkpoint. *Proc. Natl. Acad. Sci. USA.* 104:20232–20237. http://dx.doi.org/10.1073/pnas.0710519105

Kohl, T., E. Haustein, and P. Schwille. 2005. Determining protease activity in vivo by fluorescence cross-correlation analysis. *Biophys. J.* 89:2770–2782. http://dx.doi.org/10.1529/biophysj.105.061127

Kops, G.J.P.L., B.A.A. Weaver, and D.W. Cleveland. 2005. On the road to cancer: aneuploidy and the mitotic checkpoint. *Nat. Rev. Cancer.* 5:773–785. http://dx.doi.org/10.1038/nrc1714

Lan, W., and D.W. Cleveland. 2010. A chemical tool box defines mitotic and interphase roles for Mps1 kinase. *J. Cell Biol.* 190:21–24. http://dx.doi.org/10.1083/jcb.201006080

Lan, W., X. Zhang, S.L. Kline-Smith, S.E. Rosasco, G.A. Barrett-Wilt, J. Shabanowitz, D.F. Hunt, C.E. Walczak, and P.T. Stukenberg. 2004. Aurora B phosphorylates centromeric MCAK and regulates its localization and microtubule depolymerization activity. *Curr. Biol.* 14:273–286. http://dx.doi.org/10.1016/j.cub.2004.01.055

Lara-Gonzalez, P., F.G. Westhorpe, and S.S. Taylor. 2012. The spindle assembly checkpoint. *Curr. Biol.* 22:R966–R980. http://dx.doi.org/10.1016/j.cub.2012.10.006

Maciejowski, J., K.A. George, M.-E. Terret, C. Zhang, K.M. Shokat, and P.V. Jallepalli. 2010. Mps1 directs the assembly of Cdc20 inhibitory complexes during interphase and mitosis to control M phase timing and spindle checkpoint signaling. *J. Cell Biol.* 190:89–100. http://dx.doi.org/10.1083/jcb.201001050

Maeder, C.I., M.A. Hink, A. Kinkhabwala, R. Mayr, P.I.H. Bastiaens, and M. Knop. 2007. Spatial regulation of Fus3 MAP kinase activity through a reaction-diffusion mechanism in yeast pheromone signalling. *Nat. Cell Biol.* 9:1319–1326. http://dx.doi.org/10.1038/ncb1652

Maldonado, M., and T.M. Kapoor. 2011. Constitutive Mad1 targeting to kinetochores uncouples checkpoint signalling from chromosome biorientation. *Nat. Cell Biol.* 13:475–482. http://dx.doi.org/10.1038/ncb2223

Marchini, F.K., L.M.F. de Godoy, R.C.P. Rampazzo, D.P. Pavoni, C.M. Probst, F. Gnad, M. Mann, and M.A. Krieger. 2011. Profiling the *Trypanosoma cruzi* phosphoproteome. *PLoS One.* 6:e25381. http://dx.doi.org/10.1371/journal.pone.0025381

Martin-Lluesma, S., V.M. Stucke, and E.A. Nigg. 2002. Role of Hec1 in spindle checkpoint signaling and kinetochore recruitment of Mad1/Mad2. *Science.* 297:2267–2270. http://dx.doi.org/10.1126/science.1075596

Meraldi, P., V.M. Draviam, and P.K. Sorger. 2004. Timing and checkpoints in the regulation of mitotic progression. *Dev. Cell.* 7:45–60. http://dx.doi.org/10.1016/j.devcel.2004.06.006

Musacchio, A. 2011. Spindle assembly checkpoint: the third decade. *Philos. Trans. R. Soc. Lond. B Biol. Sci.* 366:3595–3604. http://dx.doi.org/10.1098/rstb.2011.0072

Musacchio, A., and E.D. Salmon. 2007. The spindle-assembly checkpoint in space and time. *Nat. Rev. Mol. Cell Biol.* 8:379–393. http://dx.doi.org/10.1038/nrm2163

Neumann, B., T. Walter, J.-K. Hériché, J. Bulkescher, H. Erfle, C. Conrad, P. Rogers, I. Poser, M. Held, U. Liebel, et al. 2010. Phenotypic profiling of the human genome by time-lapse microscopy reveals cell division genes. *Nature.* 464:721–727. http://dx.doi.org/10.1038/nature08869

Nijenhuis, W., E. von Castelmur, D. Littler, V. De Marco, E. Tromer, M. Vleugel, M.H.J. van Osch, B. Snel, A. Perrakis, and G.J.P.L. Kops. 2013. A TPR domain-containing N-terminal module of MPS1 is required for its kinetochore localization by Aurora B. *J. Cell Biol.* 201:217–231. http://dx.doi.org/10.1083/jcb.201210033

Poser, I., M. Sarov, J.R.A. Hutchins, J.-K. Hériché, Y. Toyoda, A. Pozniakovsky, D. Weigl, A. Nitzsche, B. Hegemann, A.W. Bird, et al. 2008. BAC TransgeneOmics: a high-throughput method for exploration of protein function in mammals. *Nat. Methods.* 5:409–415. http://dx.doi.org/10.1038/nmeth.1199

Reimann, J.D.R., B.E. Gardner, F. Margottin-Goguet, and P.K. Jackson. 2001. Emi1 regulates the anaphase-promoting complex by a different mechanism than Mad2 proteins. *Genes Dev.* 15:3278–3285. http://dx.doi.org/10.1101/gad.945701

Rieder, C.L., and E.D. Salmon. 1998. The vertebrate cell kinetochore and its roles during mitosis. *Trends Cell Biol.* 8:310–318. http://dx.doi.org/10.1016/S0962-8924(98)01299-9

Rieder, C.L., A. Schultz, R. Cole, and G. Sluder. 1994. Anaphase onset in vertebrate somatic cells is controlled by a checkpoint that monitors sister kinetochore attachment to the spindle. *J. Cell Biol.* 127:1301–1310. http://dx.doi.org/10.1083/jcb.127.5.1301

Rümenapp, U., A. Freichel-Blomquist, B. Wittinghofer, K.H. Jakobs, and T. Wieland. 2002. A mammalian Rho-specific guanine-nucleotide exchange factor (p164-RhoGEF) without a pleckstrin homology domain. *Biochem. J.* 366:721–728. http://dx.doi.org/10.1042/bj20020654

Santaguida, S., A. Tighe, A.M. D'Alise, S.S. Taylor, and A. Musacchio. 2010. Dissecting the role of MPS1 in chromosome biorientation and the spindle checkpoint through the small molecule inhibitor reversine. *J. Cell Biol.* 190:73–87. http://dx.doi.org/10.1083/jcb.201001036

Santaguida, S., C. Vernieri, F. Villa, A. Ciliberto, and A. Musacchio. 2011. Evidence that Aurora B is implicated in spindle checkpoint signalling independently of error correction. *EMBO J.* 30:1508–1519. http://dx.doi.org/10.1038/emboj.2011.70

Saurin, A.T., M.S. van der Waal, R.H. Medema, S.M.A. Lens, and G.J.P.L. Kops. 2011. Aurora B potentiates Mps1 activation to ensure rapid checkpoint establishment at the onset of mitosis. *Nat. Commun.* 2:316. http://dx.doi.org/10.1038/ncomms1319

Sbalzarini, I.F., and P. Koumoutsakos. 2005. Feature point tracking and trajectory analysis for video imaging in cell biology. *J. Struct. Biol.* 151:182–195. http://dx.doi.org/10.1016/j.jsb.2005.06.002

Schindelin, J., I. Arganda-Carreras, E. Frise, V. Kaynig, M. Longair, T. Pietzsch, S. Preibisch, C. Rueden, S. Saalfeld, B. Schmid, et al. 2012. Fiji: an open-source platform for biological-image analysis. *Nat. Methods.* 9:676–682. http://dx.doi.org/10.1038/nmeth.2019

Sigoillot, F.D., S. Lyman, J.F. Huckins, B. Adamson, E. Chung, B. Quattrochi, and R.W. King. 2012. A bioinformatics method identifies prominent off-targeted transcripts in RNAi screens. *Nat. Methods.* 9:363–366. http://dx.doi.org/10.1038/nmeth.1898

Stucke, V.M., H.H.W. Silljé, L. Arnaud, and E.A. Nigg. 2002. Human Mps1 kinase is required for the spindle assembly checkpoint but not for centrosome duplication. *EMBO J.* 21:1723–1732. http://dx.doi.org/10.1093/emboj/21.7.1723

Tighe, A., O. Staples, and S. Taylor. 2008. Mps1 kinase activity restrains anaphase during an unperturbed mitosis and targets Mad2 to kinetochores. *J. Cell Biol.* 181:893–901. http://dx.doi.org/10.1083/jcb.200712028

Wachsmuth, M., C. Conrad, J. Bulkescher, B. Koch, R. Mahen, M. Isokane, R. Pepperkok, and J. Ellenberg. 2015. High-throughput fluorescence correlation spectroscopy enables analysis of proteome dynamics in living cells. *Nat. Biotechnol.* 33:384–389. http://dx.doi.org/10.1038/nbt.3146

Walter, T., M. Held, B. Neumann, J.-K. Hériché, C. Conrad, R. Pepperkok, and J. Ellenberg. 2010. Automatic identification and clustering of chromosome phenotypes in a genome wide RNAi screen by time-lapse imaging. *J. Struct. Biol.* 170:1–9. http://dx.doi.org/10.1016/j.jsb.2009.10.004

Weiss, E., and M. Winey. 1996. The *Saccharomyces cerevisiae* spindle pole body duplication gene MPS1 is part of a mitotic checkpoint. *J. Cell Biol.* 132:111–123. http://dx.doi.org/10.1083/jcb.132.1.111

Westhorpe, F.G., M.A. Diez, M.D. Gurden, A. Tighe, and S.S. Taylor. 2010. Re-evaluating the role of Tao1 in the spindle checkpoint. *Chromosoma.* 119:371–379. http://dx.doi.org/10.1007/s00412-010-0261-1

Yamagishi, Y., C.-H. Yang, Y. Tanno, and Y. Watanabe. 2012. MPS1/Mph1 phosphorylates the kinetochore protein KNL1/Spc7 to recruit SAC components. *Nat. Cell Biol.* 14:746–752. http://dx.doi.org/10.1038/ncb2515

Zheng, Y. 2001. Dbl family guanine nucleotide exchange factors. *Trends Biochem. Sci.* 26:724–732. http://dx.doi.org/10.1016/S0968-0004(01)01973-9

Zhu, T., Z. Dou, B. Qin, C. Jin, X. Wang, L. Xu, Z. Wang, L. Zhu, F. Liu, X. Gao, et al. 2013. Phosphorylation of microtubule-binding protein Hec1 by mitotic kinase Aurora B specifies spindle checkpoint kinase Mps1 signaling at the kinetochore. *J. Biol. Chem.* 288:36149–36159. http://dx.doi.org/10.1074/jbc.M113.507970